ARTICLE OPEN

Check for updates

PLEKHA4 is transcriptionally regulated by *HOXD9* and regulates glycolytic reprogramming and progression in glioblastoma via activation of the *STAT3/SOCS-1* pathway

Dainan Zhang[1], Xiaoyin Wang[2], Meng Xiao[2,3], Shunchang Ma[1], Shaomin Li[2,4] and Wang Jia[1]✉

Recent studies have demonstrated that *PLEKHA4* promotes tumor growth in some cancers, such as small-cell lung cancer, melanoma, and hepatic carcinomas; however, the underlying mechanism in glioblastoma remains ambiguous. Bioinformatic was used to analysis *PLEKHA4* expression. In vitro and in vivo experiments were conducted to detect the effect of *PLEKHA4* on glioblastoma cell glycolytic reprogramming and progression. GSEA was used to analyze the signal pathways related to *PLEKHA4*. Pharmacological methods further validated the role of activation pathways. We evaluated the effects of *PLEKHA4* knockdown combined with temozolomide (TMZ) on glioblastoma cell proliferation and apoptosis in vitro and in vivo. We observed an overexpression of *PLEKHA4* in GBM cell lines, resulting in enhanced cell proliferation, inhibited apoptosis, and promoted glycolysis. Mechanistically, our study demonstrated that *PLEKHA4* mediates cell proliferation, apoptosis, and glycolysis via the *STAT3/SOCS1* signaling pathway. Additionally, *HOXD9* was predicted using Jasper, which is a transcription factor that binds to the *PLEKHA4* promoter region. Knocking down *PLEKHA4* combined with TMZ inhibited cell proliferation and promoted cell apoptosis in vitro and in vivo. Our results indicated that *HOXD9*-medicated *PLEKHA4* regulates glioblastoma cell proliferation and glycolysis via activation of the *STAT3/SOCS1* pathway.

Oncogenesis (2025)14:15 ; https://doi.org/10.1038/s41389-025-00559-0

INTRODUCTION

Malignant glioma is one of the most common primary central nervous system tumors [1–3]. Depending on their malignancies, gliomas are classified as stages I–IV [4, 5]. Glioblastoma multiforme (GBM) is most common grade IV brain glioma [6, 7]. In the past few decades, surgery has been the most common treatment for GBM, followed by chemotherapy and radiotherapy. However, patients with GBM have a high rate of postoperative recurrence and poor prognosis, leading to an average overall survival rate of approximately 1.2 years, with a small number of patients surviving for 5 years [8, 9]. Finding new molecular biomarkers can help us understand the potential mechanisms of GBM and provide new strategies for its clinical diagnosis and treatment [10, 11]. Therefore, an understanding of the proliferation and apoptosis mechanisms of GBM cells is pertinent to developing new treatment strategies.

PLEKHA4 (pleckstrin homology domain-containing family A, member 4) exists in the cell membrane and cytoplasm, and is essential for regulating intracellular signals. *PLEKHA4* reportedly regulates *DVL3* ubiquitination mediated by *CUL3-KLH12* E3 ligase, thereby regulating the Wnt signaling [12–14]. *PLEKHA4* exhibits higher expression in melanomas than in healthy melanocytes [15]. There are reports showing that *PLEKHA4* regulated cell growth, apoptosis, metastasis, and invasion in various malignant cancers, which may affect the prognosis in these patients. However, the role of *PLEKHA4* in GBM biological processes remains unknown. To investigate whether *PLEKHA4* could be a potential target in GBM treatment, further research on its role and potential mechanisms of action in GBM crucial. The purpose of our study is to explore the role of *PLEKHA4* in GBM progression.

In our study, *PLEKHA4* was highly expressed in GBM cells and was observed to enhance cell proliferation, inhibit cell apoptosis, and promote cell glycolytic reprogramming including glucose uptake and ATP and lactate content in vitro. Additionally, *PLEKHA4* promoted the growth of GBM tumors in nude mice. Mechanistically, the findings indicated that *HOXD9* bound to the promoter of *PLEKHA4*, which was discovered to regulate cell proliferation, apoptosis, and glycolysis in GBM cells and promote GBM progression, which in turn activated the *STAT3/SOCS1* pathway. Additionally, it was observed that knockdown of *PLEKHA4* combined with temozolomide (TMZ) treatment had a higher therapeutic effect on inhibiting cell proliferation, promoting cell glycolysis in vitro, and inhibiting tumor growth in vivo than knocking down *PLEKHA4* or TMZ treatment alone, indicating that *PLEKHA4* could promote TMZ sensitivity. In conclusion, these findings reveal the underlying mechanism of *PLEKHA4* in regulating GBM cell glycolysis and indicate a potential new target for GBM treatment.

[1]Department of Neurosurgery, Beijing Tian Hospital, Beijing Neurosurgical Institute, Capital Medical University, Beijing, China. [2]Henan Key Laboratory of Neurorestoratology, The First Affiliated Hospital of Xinxiang Medical University, Weihui, Henan, China. [3]Graduate School of Beijing University of Chinese Medical, Beijng, China. [4]Ann Romney Center for Neurologic Diseases, Department of Neurology, Brigham and Women's Hospital and Harvard Medical School, Boston, MA, USA. ✉email: noanswear@hotmail.com

Received: 29 July 2024 Revised: 11 April 2025 Accepted: 29 April 2025
Published online: 09 May 2025

RESULTS

PLEKHA4 is overexpressed in GBM tissues

To investigate whether *PLEKHA4* was highly expressed, expression in GBM was compared to that in non-tumor tissues. TCGA results revealed that *PLEKHA4* expression was considerably higher in GBM tissues (Fig. 1A, B) than in non-tumor tissues. To further detect *PLEKHA4* expression in GBM cells, *PLEKHA4* expression was analyzed in human GBM cells (U87, U251, U343, and T98G) and human brain microvascular endothelial cells (HBMECs). *PLEKHA4* was highly expressed in all GBM cells compared with HBMECs (Fig. 1C, D). Bioinformatics analysis and validation in GBM cells indicated that *PLEKHA4* was highly expressed in GBM cells.

PLEKHA4 regulates cell growth and apoptosis in vitro

According to the expression of *PLEKHA4* in the human glioma cells (U87, U251, U343, and T98G) and HBMECs, we selected the T98G and U87cells for sh*PLEKHA4* or *PLEKHA4* overexpression studies. A lentivirus packaged with three different sh*PLEKHA4* constructs was transfected into T98G cells to down-regulate mRNA and protein expression (Fig. 2A, B). The results indicated that the knockdown efficiency of sh*PLEKHA4-1* and sh*PLEKHA4-3* was relatively high; therefore, sh*PLEKHA4-1* and sh*PLEKHA4-3* were selected for cell functional experiments because of their superior knockdown efficiency. Simultaneously, a lentivirus harboring the *PLEKHA4* was transfected into U87 cells to overexpress *PLEKHA4* (Fig. 2C, D).

The CCK8 assay was performed to examine cell proliferation. The results revealed that the down-regulation of *PLEKHA4* inhibited T98G cell proliferation (Fig. 2E), and overexpression of *PLEKHA4* promoted U87 cell proliferation (Fig. 2F). Cell apoptosis was further investigated using flow cytometry. The results illustrated that the amount of apoptotic cells among the PLEKHA4-knockout group was markedly higher than that in the control group (26.43 ± 0.79% for sh*PLEKHA4-1*, 29.44 ± 1.02% for sh*PLEKHA4-3*, and 5.43 ± 0.34% for shNC). Moreover, *PLEKHA4* overexpression notably reduced the percentage of apoptotic cells in U87 cells (3.29 ± 0.25% for *PLEKHA4* overexpression, 6.51 ± 0.03% for Vector group) (Fig. 2G, H). These findings suggest that *PLEKHA4* regulates GBM cells proliferation and apoptosis.

PLEKHA4 elevates glucose uptake, lactate production, and ATP content

It has been reported that glycolysis could mediate the growth of lung and breast cancer cells [16, 17]. In this study, we explored the changes in GBM glycolysis regulated by *PLEKHA4*. The glucose uptake, lactate production in the cell supernatant, and ATP content-related biochemical alterations were assessed to evaluate whether *PLEKHA4* mediated glycolysis in GBM cells. The knockdown of *PLEKHA4* was reported to reduce glucose uptake, lactate, and ATP content distinctly in T98G cells, whereas overexpressing *PLEKHA4* in U87 cells escalated glucose uptake, lactate, and ATP content (Fig. 2I–K). Collectively, these results demonstrated that *PLEKHA4* regulates glycolytic reprogramming in GBM cells.

We further investigated whether *PLEKHA4*-dependent glycolysis in GBM cells affects cell proliferation and apoptosis. *PLEKHA4*-overexpressing U87 cells were treated with 25 μM of 2-Deoxy-D-glucose (2-DG; MCE, USA), a glycolysis inhibitor, to evaluate cell proliferation and apoptosis. The CCK8 assay detected cell proliferation (Fig. 3A), which indicated that overexpressing *PLEKHA4* promoted GBM cell growth, while 2-DG could inhibit the promotion effect mediated by

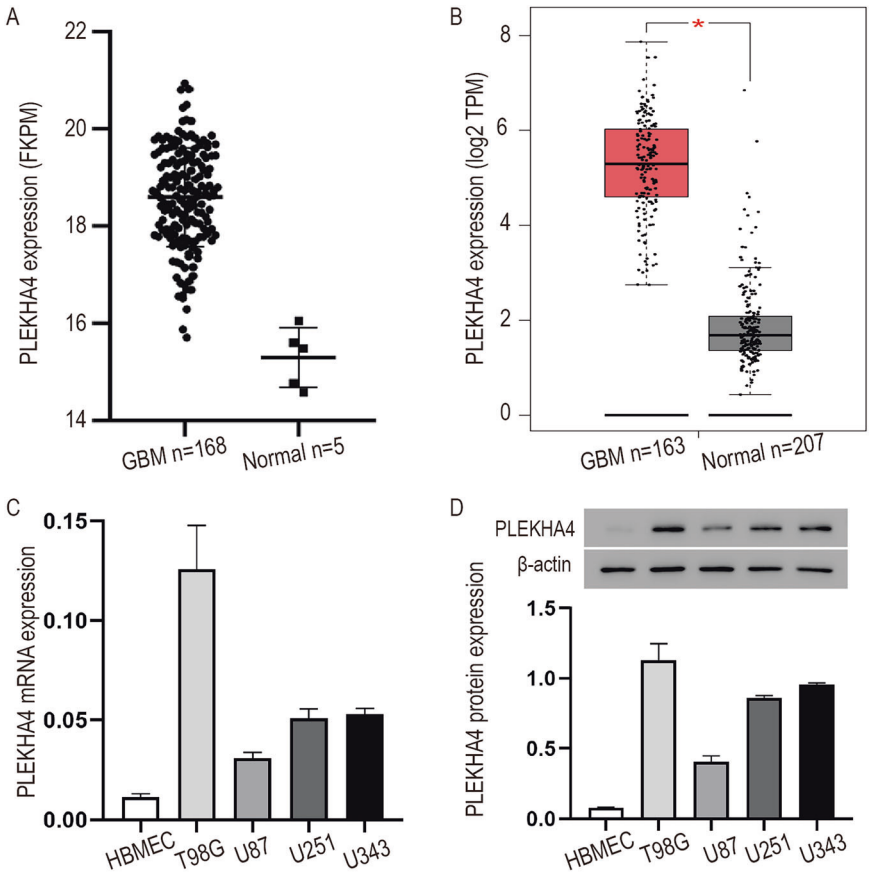

Fig. 1 *PLEKHA4* is highly-expressed in the TCGA database and GBM cells. A *PLEKHA4* is higher in GBM tissues ($n = 168$) than in non-tumor tissues (Normal $n = 5$) at the mRNA level. **B** *PLEKHA4* is higher in GBM tissues ($n = 163$) than in non-tumor tissues ($n = 207$). **C** *PLEKHA4* level in GBM cells by qRT-PCR. **D** Western blot detected *PLEKHA4* in cells. The above qPCR and Western blot experiments were conducted using cell extracts from three independent cultures, with two replicates conducted each time.

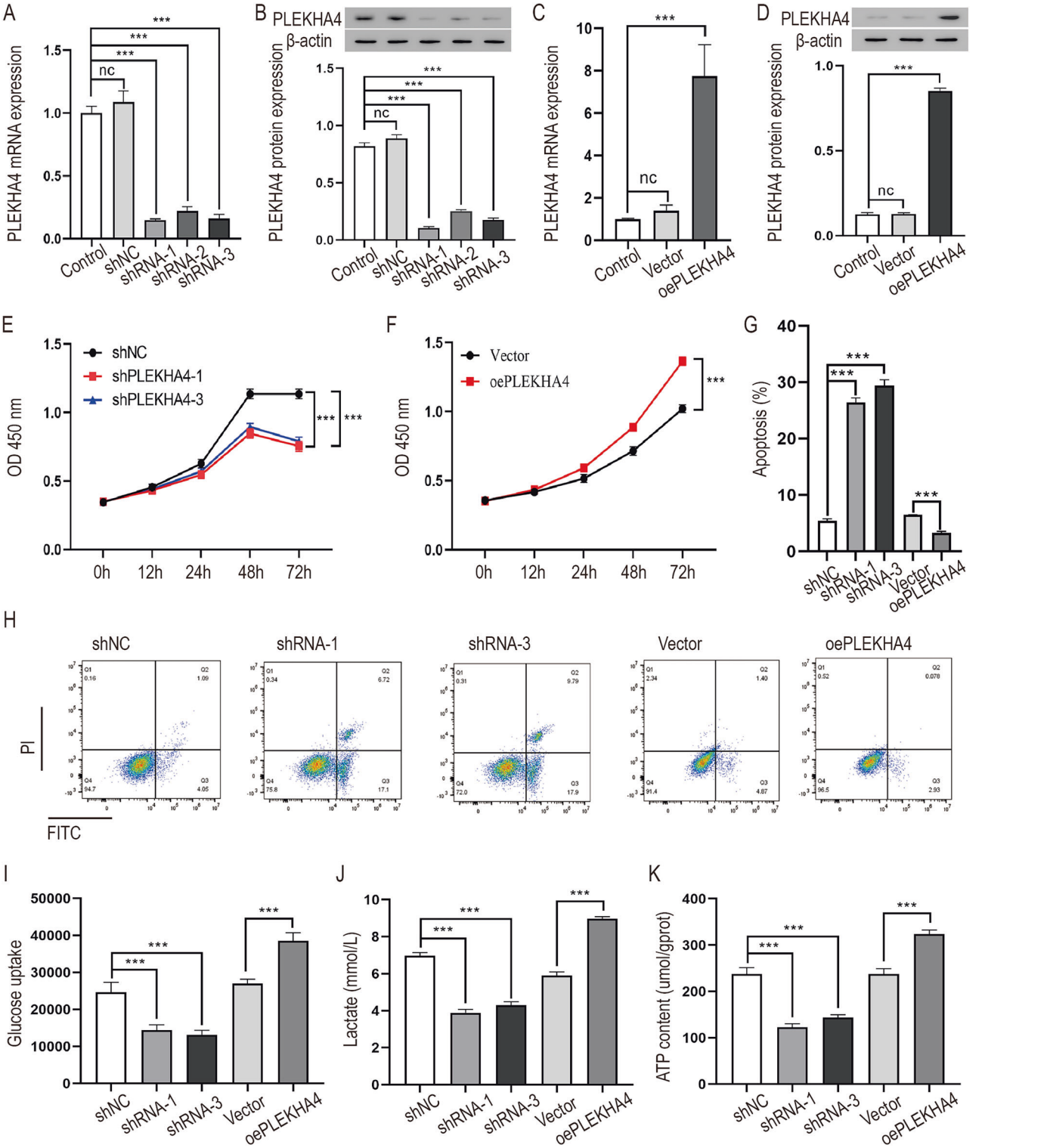

Fig. 2 ***PLEKHA4* affects GBM cells proliferation and apoptosis in vitro.** Experiments employed knockdown of *PLEKHA4* (shRNA-1, shRNA-2, shRNA-3) or shNC in T98G cells and overexpression of *PLEKHA4* (oe*PLEKHA4*) or vector in U87 cells were for subsequent experiments. **A**, **B** *PLEKHA4* was down-regulated in sh-RNA targeting the *PLEKHA4* group, ***$p < 0.001$. **C**, **D** *PLEKHA4* was up-regulated in the overexpression PLEKHA4 group. ***$P < 0.001$. **E**, **F** CCK8 assay indicated that the knockdown of *PLEKHA4* inhibited U87 cell growth, and vice versa. ***$p < 0.001$ vs. NC groups. **G**, **H** The apoptotic cells were measured, and quantitative results are expressed as mean ± SD. ***$p < 0.01$. **I** Glucose uptake assays, **J** lactate production, and **K** ATP content were detected in T98G cells with knockdown of *PLEKHA4* or U87 cells with *PLEKHA4* overexpression. ***$p < 0.001$. The cell experiments were conducted from three independent cultures, with two replicates conducted each time.

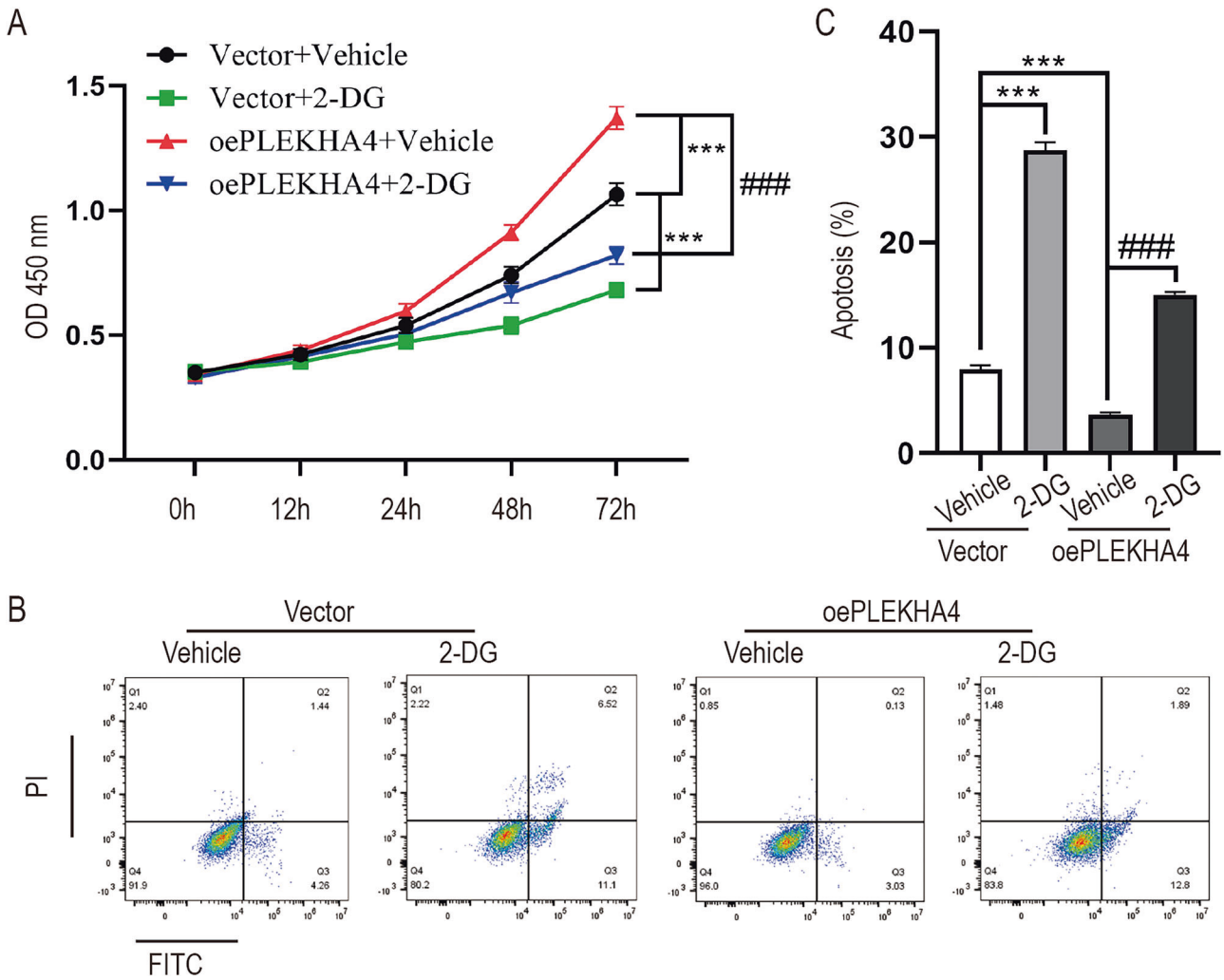

Fig. 3 *PLEKHA4* overexpression protects glioma cells from apoptosis induced by glycolysis inhibitor 2-DG. The U87 cells were treated with overexpression of *PLEKHA4*, combined with 25 μM of the Glycolysis inhibitor 2-DG. **A** CCK8 assay detected cell viability, $^{**}p < 0.01$, $^{***}p < 0.001$, $^{###}p < 0.001$. **B** The apoptotic cells were detected. **C** The quantitative results were presented, $^{***}p < 0.001$, $^{###}p < 0.001$. The cell experiments were conducted three independent cultures, with two replicates conducted each time.

the overexpression of *PLEKHA4*. Subsequently, the apoptotic cells were examined using flow cytometry (Fig. 3B). The percentage of apoptotic cells decreased considerably (Fig. 3C, 3.67 ± 0.22% for overexpression of *PLEKHA4*, 7.92 ± 0.40% for the Vector group), whereas 2-DG reversed the *PLEKHA4* overexpression-induced reduction in the percentage of apoptotic U87 cells (15.06 ± 0.25% for *PLEKHA4* overexpression cells treated with 2-DG, 28.76 ± 0.75% for the 2-DG-treated Vector group). These results suggest that 2-DG suppresses *PLEKHA4* overexpression-mediated cell proliferation and apoptosis.

PLEKHA4 activates the *STAT3* pathway to regulate cell growth, apoptosis, and glycolysis

GSEA showed a positive correlation between *PLEKHA4* and the *STAT3* pathway (Fig. 4A). The *STAT3* pathway regulates cell growth and apoptosis in various types of cancer. We speculate that *PLEKHA4* affects GBM proliferation, apoptosis, and glycolysis by modulating the *STAT3* pathway. The expression of phosphorylated *STAT3* in *PLEKHA4*-knockout T98G cells was decreased, whereas that of *SOCS1* in *PLEKHA4*-knockout T98G cells was increased. The opposite result was obtained in *PLEKHA4*-overexpressing U87 cells; nonetheless, the total *STAT3* concentration in the two treatment groups remained constant (Fig. 4B, C).

To further explore the mechanism underlying *PLEKHA4*-mediated regulation, the *STAT3* inhibitor AG490 was used to suppress the *STAT3* pathway. Consequently, AG490 inhibited the up-regulation of *STAT3* induced by *PLEKHA4* overexpression in U87 cells (Fig. 4D, E). CCK8 assays revealed that AG490 inhibited *PLEKHA4* overexpression mediated U87 cell proliferation (Fig. 4F). Annexin V-FITC staining demonstrated that AG490 treatment increased the percentage of apoptosis in U87 cells (28.26 ± 0.72) as compared to that of the vehicle group (7.45 ± 0.31); similarly, the apoptosis inhibition inducted by *PLEKHA4* overexpression was also alleviated by AG490 treatment (16.43 ± 1.32) compared with vehicle-treated *PLEKHA4*-overexpressing cells (4.03 ± 0.25). These results demonstrated that AG490 reversed the *PLEKHA4* overexpression-induced inhibition of apoptosis of U87 cells (Fig. 4G, H). Furthermore, AG490 reversed the decrease in glucose uptake and lactate and ATP content mediated by *PLEKHA4* overexpression in U87 cells (Fig. 4I–K). Therefore, these findings suggest that *PLEKHA4* regulates proliferation, apoptosis, and glucose, lactate, and ATP levels in GBM cells by activating the STAT3 pathway.

PLEKHA4 regulates GBM cell growth, apoptosis, and glycolysis by directly activating the transcription of *HOXD9*

The purpose of this study was to investigate the molecular mechanisms by which *PLEKHA4* participates in cell proliferation, apoptosis and glycolysis. The transcription factors of *PLEKHA4*

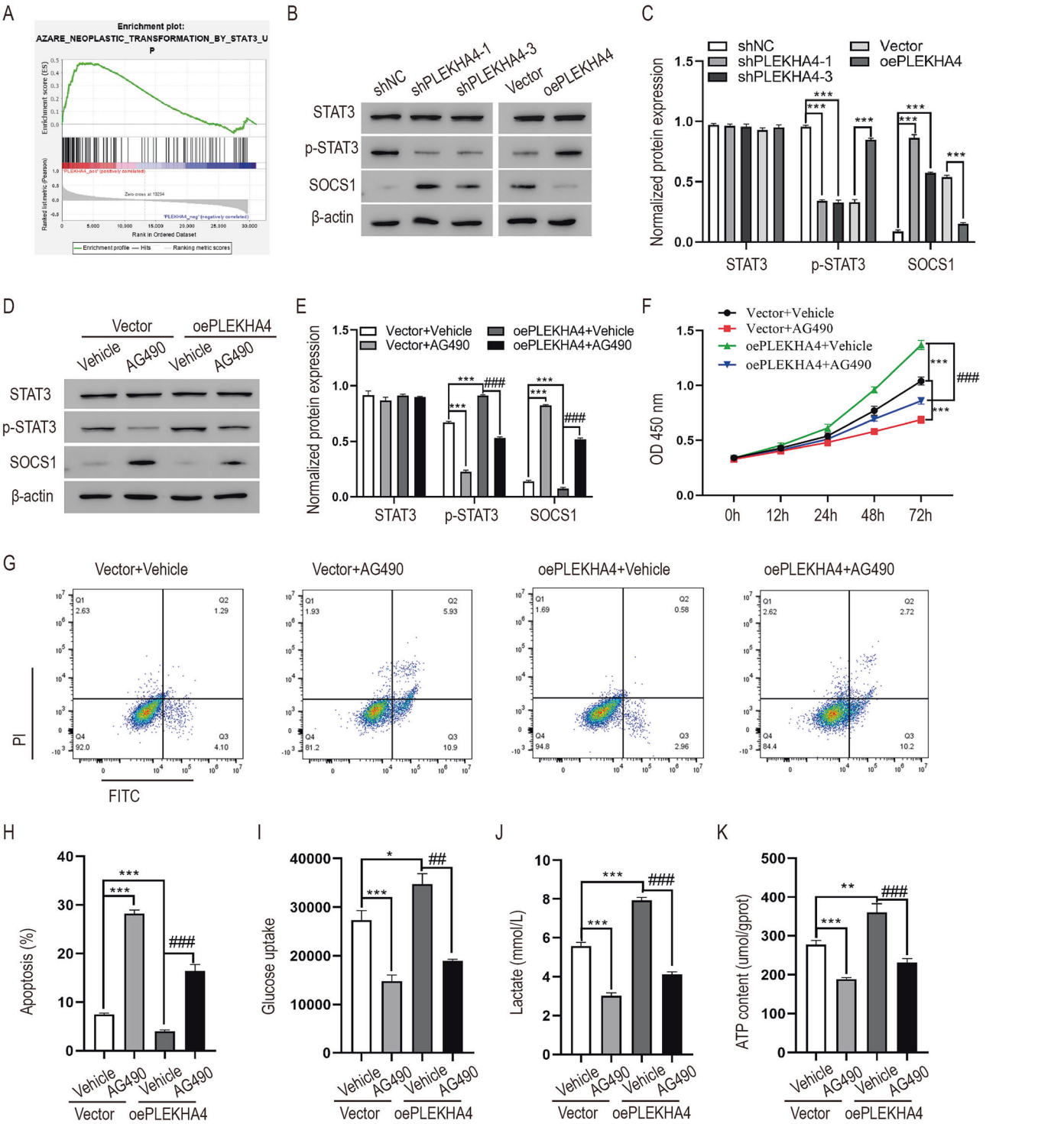

Fig. 4 ***PLEKHA4*** **regulated GBM cell proliferation and apoptosis through the** ***STAT3*** **pathway. A** GSEA showed that *PLEKHA4* regulated GBM cell growth and apoptosis through the *STAT3* pathway. **B** Western blot detected *STAT3* pathway related proteins, *STAT3*, *p-STAT3* and *SOCS1*. **C** Quantitative analysis of *STAT3* pathway-related proteins, ***$p < 0.001$. The U87 cells with overexpression of *PLEKHA4* combined with 10 μM *STAT3* inhibitor AG490. **D**, **E** Western blot detected the *STAT3* pathway-related proteins in U87 cells. ***$p < 0.001$ compared with Vector + Vehicle group, ###$p < 0.001$ compared with oe*PLEKHA4* + Vehicle group. **F** CCK8 detected the U87 cells growth. ***$p < 0.001$ compared with Vector + Vehicle group, ###$p < 0.001$ compared with oe*PLEKHA4* + Vehicle group. **G** Apoptotic cells were analyzed by flow cytometry. **H** The quantitative results were presented. **I** Glucose uptake assays, **J** lactate production, and **K** ATP production were measured, ***$P < 0.001$ compared with Vector +Vehicle group, ##$p < 0.01$, ###$p < 0.001$ compared with oe*PLEKHA4* + Vehicle group. The cell experiments were conducted three independent cultures, with two replicates conducted each time.

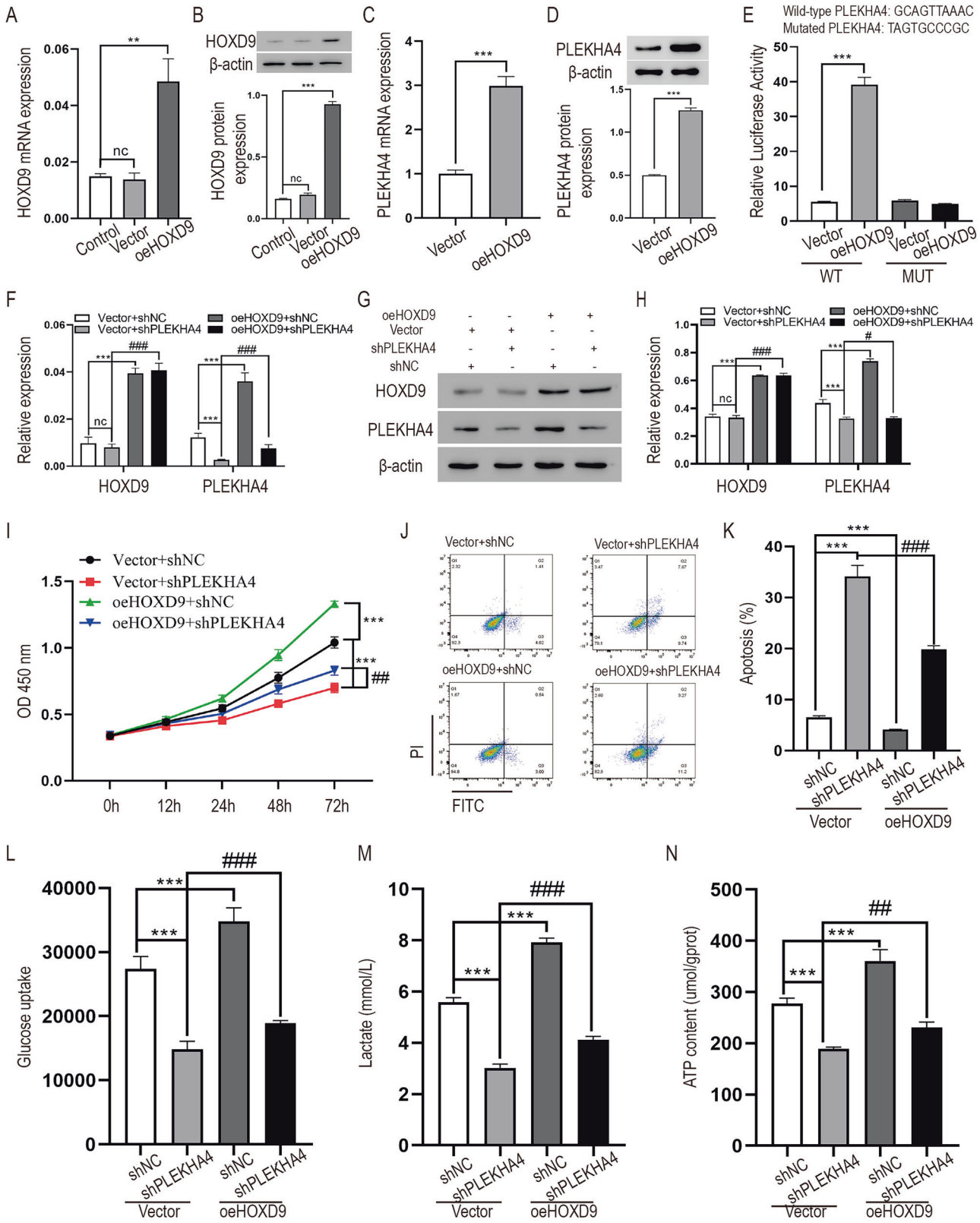

were predicted using JASPAR (https://jaspar.genereg.net), and *HOXD9* was selected for subsequent research through the analysis of the hypothesized results and references. *HOXD9* expression at the mRNA and protein levels was detected by overexpressing *HOXD9* in U87 cells (Fig. 5A, B). Next, we investigated the effect of *HOXD9* on *PLEKHA4* expression, and the results indicated that overexpressing *HOXD9* promoted *PLEKHA4* expression (Fig. 5C, D). Here, we constructed WT-*PLEKHA4* promoter and MUT-*PLEKHA4* promoter and co-transfected them with *HOXD9* overexpression into U87 cells. Then, we detected the activity of the *PLEKHA4*

Fig. 5 *HOXD9* regulates glioma cells proliferation, apoptosis, glucose uptake and aerobic glycolysis. *HOXD9* expression in U87 cells transfected with the vector or *HOXD9* overexpression. **A** The mRNA was quantified. **B** The protein was quantified. $^{**}p < 0.01$, $^{***}p < 0.001$. **C** qRT-PCR detected the mRNA expression of *PLEKHA4*, $^{***}p < 0.001$. **D** Western Blot detected the protein expression of *PLEKHA4*, $^{***}p < 0.001$. **E** Luciferase reporter assay shows that *HOXD9* binds to *PLEKHA4*, $^{***}p < 0.001$. The luciferase reporter plasmid containing WT or MUT-*PLEKHA4* was co-transfected into U87 cells with *HOXD9* overexpression or vector. **F** The mRNA, and **G**, **H**. The protein expression levels of *HOXD9* and *PLEKHA4* in U87 cells co-transfected with sh*PLEKHA4* and *HOXD9* overexpression. $^{***}p < 0.001$ compared with Vector + shNC, $\#p < 0.05$, $\#\#\#p < 0.001$ compared with Vector + sh*PLEKHA4* group. **I** CCK-8 detected the activity of the U87 cells. $^{***}p < 0.001$ compared with Vector + shNC group, $\#\#\#p < 0.001$ compared with Vector + sh*PLEKHA4* group. **J**, **K** Flow cytometry detected apoptosis. $^{***}p < 0.001$ compared with Vector + shNC group, $\#\#\#p < 0.001$ compared with Vector + sh*PLEKHA4* group. **L** Glucose uptake assays, **M** lactate production, **N** ATP production were measured, $^{***}p < 0.001$ compared with Vector + shNC group, $\#\#p < 0.01$, $\#\#\#p < 0.001$ compared with Vector + sh*PLEKHA4* group. The cell experiments were conducted three independent cultures, with two replicates conducted each time.

promoter, and analyzed the effect of *HOXD9* on the *PLEKHA4* promoter using luciferase (Fig. 5E). To further verify whether *HOXD9* regulates *PLEKHA4*-mediated glycolysis, we overexpressed *HOXD9* alone or with *PLEKHA4* knockdown with simultaneous transfected into U87 cells, and *HOXD9* and *PLEKHA4* expression at the mRNA level was detected using qRT-PCR (Fig. 5F). Western blot was used to analyze *HOXD9* and *PLEKHA4* levels (Fig. 5G, H). CCK8 results showed that *HOXD9* overexpression promoted cell growth, whereas knockdown of *PLEKHA4* inhibited cell growth (Fig. 5I). Apoptosis results showed that *HOXD9* overexpression inhibited apoptosis induced by *PLEKHA4* knockdown (Fig. 5J–K). We also found that *HOXD9* overexpression promoted glycolysis and lactate and ATP contents, which were inhibited by *PLEKHA4* knockdown (Fig. 5L–N). These results suggest that *HOXD9* mediates *PLEKHA4*-induced cell proliferation, apoptosis, and glycolysis.

Knocking down *PLEKHA4* suppresses tumor growth in vivo

In vivo experiments were conducted to verify the effect of *PLEKHA4* on the growth of GBM tumors. T98G shNC, T98G sh*PLEKHA4-1*, and T98G sh*PLEKHA4-3* cells were subcutaneously administered into the mouse models, and the shNC group had the fastest tumor growth rate (Fig. 6A, B). The tumor size in the shNC group was also the largest (Fig. 6C). Additionally, the tumor weights were substantially lighter than those in the shNC group (Fig. 6D). Western blot and qPCR displayed *PLEKHA4* expression in the tumor tissues (Fig. 6E–G), which suggested that *PLEKHA4* suppressed GBM tumorigenesis in vivo.

Overexpression *PLEKHA4* promotes tumor growth via *STAT3* in intracranial model

To verify the effect of *PLEKHA4* on the growth of GBM tumors, U87-vector, U87-oe*PLEKHA4* cells were injected into the brain of nude mice in situ. The results showed that overexpression *PLEKHA4* promoted tumor growth, while *STAT3* inhibitor AG490 inhibited tumor growth, while overexpression *PLEKHA4* in combination with AG490 could inhibited tumor growth (Fig. 7A). Immunofluorescence was used to analyze the expression of *Ki67* in brain sections, and the results showed that overexpression promoted *Ki67* expression, while *STAT3* inhibitor AG490 inhibited *Ki67* expression, overexpression *PLEKHA4* combined with *STAT3* inhibitor AG490 inhibited *Ki67* expression (Fig. 7B). Overall, these results showed that overexpression *PLEKHA4* promoted tumor growth in intracranial model, *STAT3* inhibitor AG490 could reverse this promoting effect. Overexpression *PLEKHA4* promoted tumor growth via *STAT3* in vivo.

TMZ combined with knocking down *PLEKHA4* promoted cell apoptosis in vitro

We investigated whether TMZ in could play a role in *PLEKHA4* mediated cell apoptosis in vitro. After treatment with different concentrations of TMZ, the results showed that the IC 50 in the T98G cells with *PLEKHA4* knockdown was significantly reduced, (shNC: IC 50 = 274.9; sh*PLEKHA4*: IC 50 = 175.8, Fig. 8A). The flow cytometry results indicated that TMZ promoted T98G cells apoptosis (37.8 ± 0.21), *PLEKHA4* knockdown promoted T98G cells apoptosis (26.7 ± 1.62), and TMZ combined with *PLEKHA4* knockdown enhanced the effect of promoting apoptosis (65.95 ± 0.56), compared with the control group (3.7 ± 0.64) (Fig. 8B, C). TMZ has been used as a therapeutic drug for adult malignant glioblastoma, mainly exerting anti-tumor effects through DNA damage. Immunofluorescence detection of *γ-H2AX* was used to evaluate DNA damage. We observed an increase in DNA damage in sh*PLEKHA4* cells after TMZ treatment, and in the absence of TMZ, *PLEKHA4* knockdown had very little effect on DNA damage (Fig. 8D). These results indicate that *PLEKHA4* enhances TMZ treatment-induced DNA damage and promotes cell apoptosis.

TMZ combined with *PLEKHA4* knockdown inhibits tumor growth in vivo

To evaluate the effect of *PLEKHA4* on the TMZ-resistant phenotype in vivo, T98G-shNC or T98G-sh*PLEKHA4* cells were injected into nude mice. The results indicated that TMZ inhibited tumor growth, knocking down *PLEKHA4* inhibited tumor growth, and knocking down *PLEKHA4* combined with TMZ could significantly inhibit tumor growth (Fig. 9A, B). Additionally, comparing the tumors of each group, it was found that the tumor in the *PLEKHA4* knockdown combined with the TMZ group was the smallest (Fig. 9C), and the tumor weight was the lightest (Fig. 9D). The HE staining results showed a significant decrease in cell density in the *PLEKHA4* knockdown combined with the TMZ group (Fig. 9E). Tunel staining was used to analyze cell apoptosis in the transplanted tumor specimens, and the results showed an increase in the number of apoptotic cells (Fig. 9F, G). Overall, these results indicate that *PLEKHA4* promotes glioma cell resistance to TMZ in vivo.

Further investigate the effect of *PLEKHA4* on the TMZ-resistance phenotype in vivo, U87-shNC or U87-sh*PLEKHA4* cells were injected into the brain of nude mice. The results showed that TMZ inhibited tumor growth, knockdown *PLEKHA4* also inhibited tumor growth, knockdown *PLEKHA4* in combination with TMZ significantly inhibited tumor growth (Fig. 10A). Immunofluorescence was used to analyze the expression of *Ki67* in brain sections, and the results showed that knockdown *PLEKHA4* combined with TMZ significantly inhibited the expression of *Ki67* (Fig. 10B). Overall, these results indicated that *PLEKHA4* promotes resistance of glioma cells to TMZ in intracranial models.

DISCUSSION

GBM is the most prevalent and aggressive tumor in the central nervous system [1, 18]. Owing to its remarkable tolerance for complex and adverse environments, GBM is notoriously challenging to treat and prognosticate and has a tendency for recurrence [19]. Glycolysis plays a crucial role in adapting GBM cells to various environmental conditions; consequently, GBM cells require more glucose than normal glial cells to maintain cell proliferation. Glucose provides carbon and nitrogen precursors for lipid and DNA synthesis in GBM cells by entering glycolysis and maintaining cell redox homeostasis (known as the Warburg effect) [20]. Studies have reported that the metabolites of aerobic glycolysis can

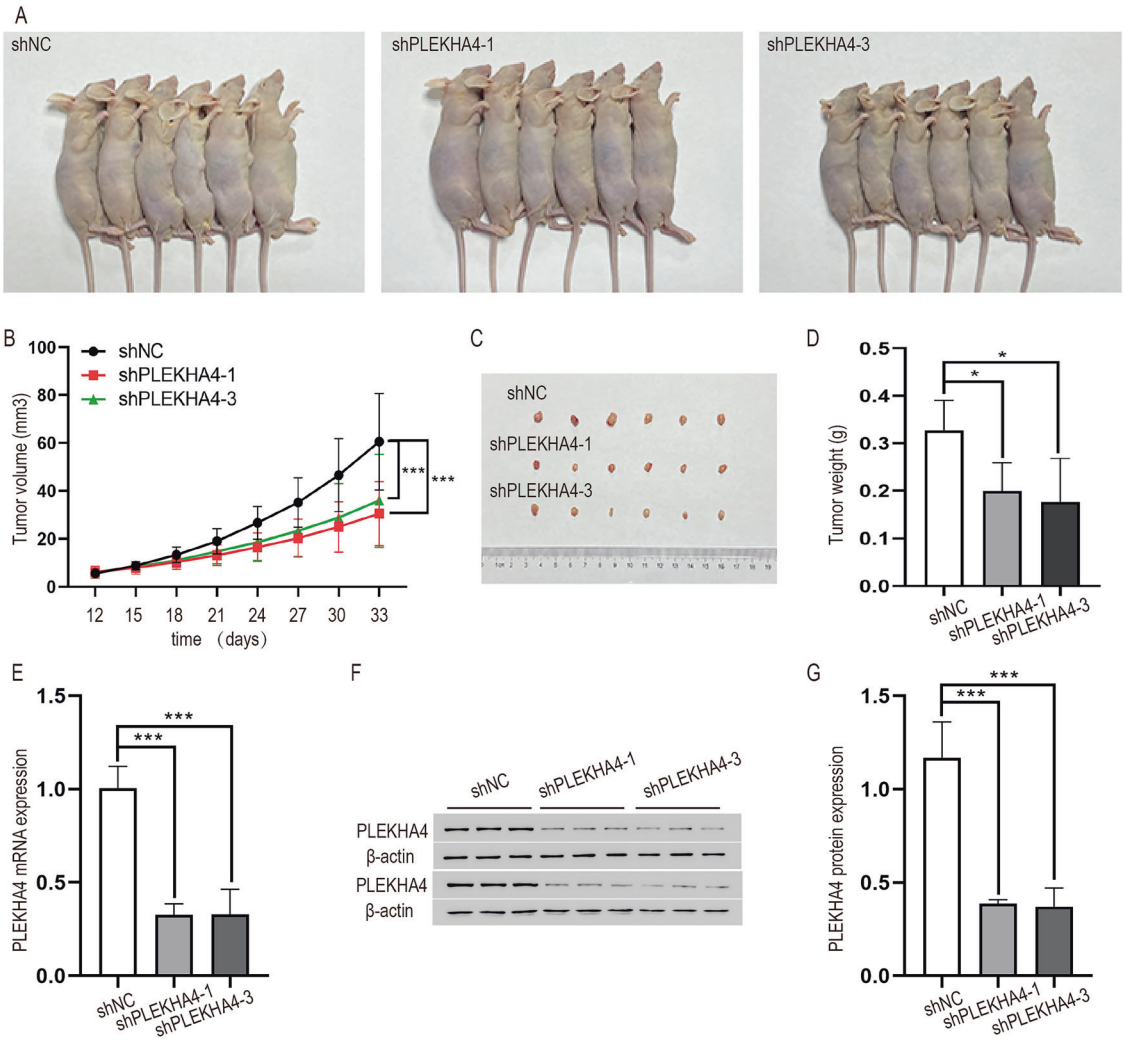

Fig. 6 Knocking down *PLEKHA4* inhibits GBM tumor growth in vivo. A Nude mice xenograft images. **B** Tumor growth curve, ***$p < 0.001$ compared with shNC group. **C** Tumor size, and **D** tumor weights were presented, *$p < 0.05$ compared with shNC group. **E** *PLEKHA4* was analyzed in tumor tissues by qPCR, ***$p < 0.001$ compared with shNC group. **F**, **G** *PLEKHA4* expression and normalized *PLEKHA4* protein expression were presented in tumor tissues. ***$p < 0.001$ compared with shNC group.

interrupt the infiltration of immune cells and suppress their anti-tumor properties [21, 22]. Therefore, targeted therapy for glycolytic abnormalities could emerge as a potential therapeutic strategy for GBM.

PLEKHA4 is a multi-domain adaptor protein [12] that is overexpressed in certain tumors and facilitates the prognosis of cancers [13, 15]. However, there is limited research on whether PLEKHA4 can regulate the progression of GBM. Then, "gain and loss" strategies were used to discover that PLEKHA4 promoted GBM cell proliferation, while suppressing cell apoptosis. PLEKHA4 knock-down considerably reduced glucose uptake, lactate production, and ATP content. Blocking glycolysis using the glycolytic inhibitor 2-DG in U87 cells, resulted in a *PLEKHA4* overexpression mediated promotion of cell proliferation and reversal of cell apoptosis inhibition.

Previous studies have demonstrated that STAT3 interacts with other cell-signaling pathways, such as NF-κB in tumor cells, imparting robustness for tumor progression [23–25]. *STAT3* is activated in tumor cells and is involved in cell proliferation, metastasis, apoptosis, and angiogenesis [23, 26]. The impact of *PLEKHA4* in activating the *STAT3/SOCS1* pathway in U87 cells was validated. Additionally, the involvement of the *STAT3/SOCS1* pathway in *PLEKHA4*-overexpressing cells was detected using the STAT3 inhibitor AG490. AG490 evidently weakened cell proliferation and glycolysis, along with dampening apoptosis induced by *PLEKHA4* overexpression. The above results indicated that *PLEKHA4* might regulate cell proliferation, apoptosis and glycolysis by activating the *STAT3/SOCS1* pathway.

In addition, *STAT3* signaling pathway may be associated with cell migration and invasion in GBM [27, 28], and our study also found that *STAT3* signaling pathway is downstream of *PLEHA4*. Therefore, we speculate that *PLEKHA4* may also be involved in regulating the migration and invasion of GBM cells. In this study, we found that overexpression *PLEKHA4* promotes tumor growth in intracranial models, while *STAT3* inhibitor AG490 could reverse this trend. In summary, the above results indicate that *PLEKHA4* regulates the progression of gliomas through *STAT3* pathway.

Homeobox D9 (*HOXD9*) is associated with the development of many malignant tumors, sunch as GBM and ovarian and cervical cancer [29–31]. Previous studies have demonstrated that *HOXD9* promotes gastric cancer cell invasion, and metastasis through the *RUN* and *EYVE* domains [31]. *HOXD9* transcriptionally activates *HMCN1*, which facilitates cervical cancer progression [32]. *HOXD9* is a transcription factor for *PLEKHA4* as predicted by JASPAR. However, studies on the effect of *HOXD9* in GBM are limited. We hypothesized that *PLEKHA4* was regulated by *HOXD9* in GBM. In

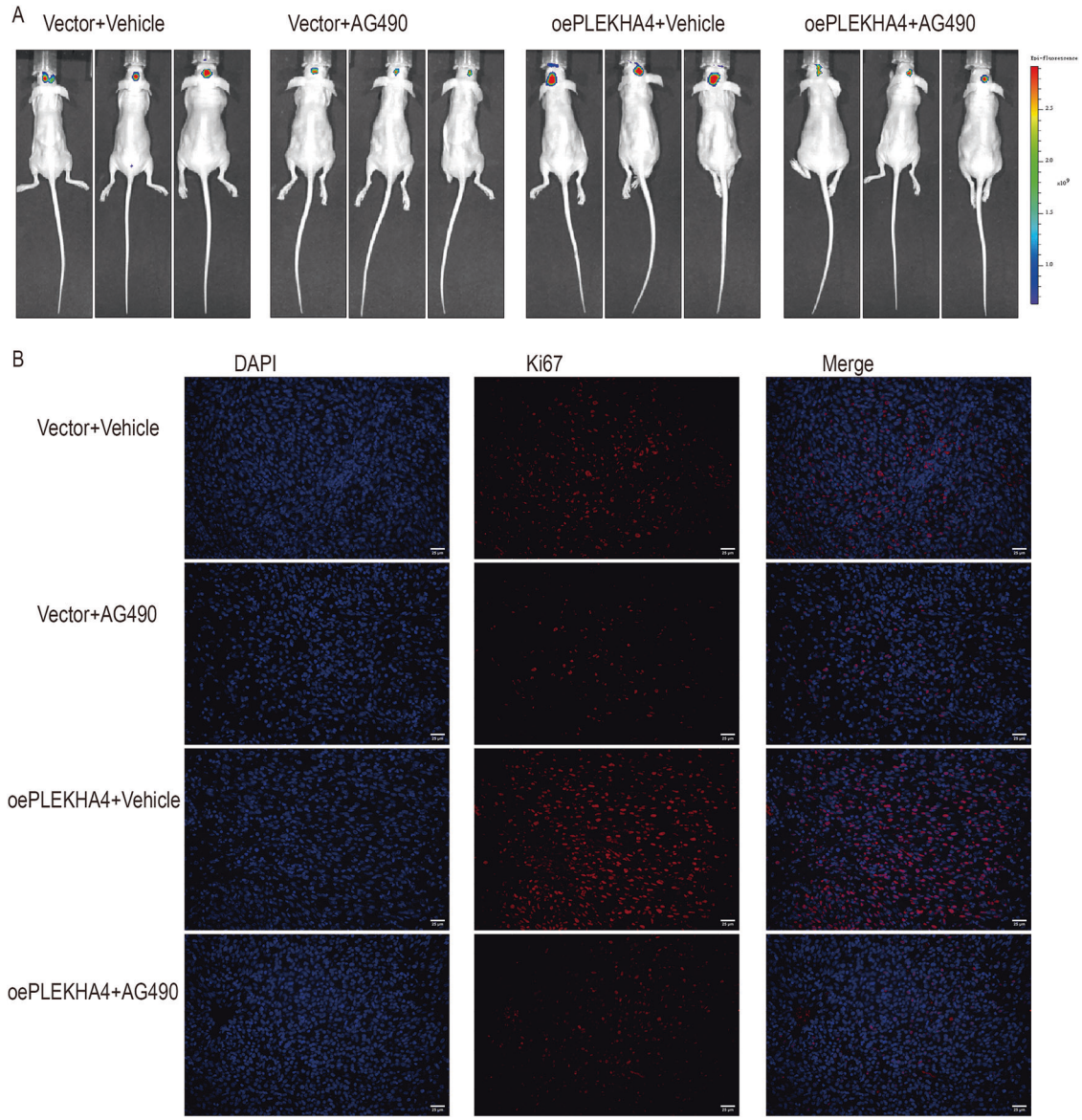

Fig. 7 Overexpression *PLEKHA4* promotes tumor growth in intracranial model. A The image of intracranial tumors. **B** Immunofluorescence detected the expression of *Ki67* (400×).

our study, the findings revealed that *HOXD9* promoted the transcription of *PLEKHA4* by binding to its promoter site. Through *HOXD9* overexpression in U87 cells, we found that *PLEKHA4* became highly expressed, while knocking down *PLEKHA4* did not affect the expression of *HOXD9*. In addition, *HOXD9* could restore cell proliferation and glycolysis regulated by knocking down *PLEKHA4* in U87 cells. The above results indicate that the *HOXD9–PLEKHA4* axis could regulate glycolysis and GBM development.

TMZ is an alkylating agent with anti-tumor activity, mainly used for recurrent or progressive GBM or anaplastic astrocytoma after conventional treatment [33, 34]. A previous study indicated that lncRNA *PDIA3P1* was highly expressed in TMZ-resistant GBM cells, and promoted TMZ resistance in glioma [35]. Another study reported that *ALDH3P1* was lowly expressed in TMZ-resistance glioblastoma cells [36]. In our study, we demonstrated the effectiveness of *PLEKHA4* knockdown combined with TMZ treatment in vitro and in vivo, revealing that *PLEKHA4* could promote TMZ sensitivity. This study provided a new strategy for the treatment of glioma, showing that *PLEKHA4* knockdown combined with TMZ has a better inhibitory effect on cell proliferation and tumor growth than knocking down *PLEKHA4* or TMZ treatment alone.

In conclusion, we found that *PLEKHA4* is more highly expressed in GBM cells and promotes GBM development. *HOXD9* directly promotes the transcription of *PLEKHA4* and activates the STAT3/SCOS1 pathway to regulate cell glycolysis and promote GBM progression. Additionally, the combination of *PLEKHA4* knockdown and TMZ has a better anti-tumor effect than TMZ treatment or *PLEKHA4* knockdown alone both in vitro and in vivo. Our research results demonstrate the biological roles of *PLEKHA4* under pathological conditions in GBM, explain the potential mechanism of GBM glycolysis, and determine that *PLEKHA4* may be a potential therapeutic target in GBM.

MATERIALS AND METHODS

Bioinformatic analysis

The data for human glioma tissues were downloaded from TCGA (The Cancer Genome Atlas, http://tcga-data.ncbi.gov/tvga/) and GEPIA (Gene

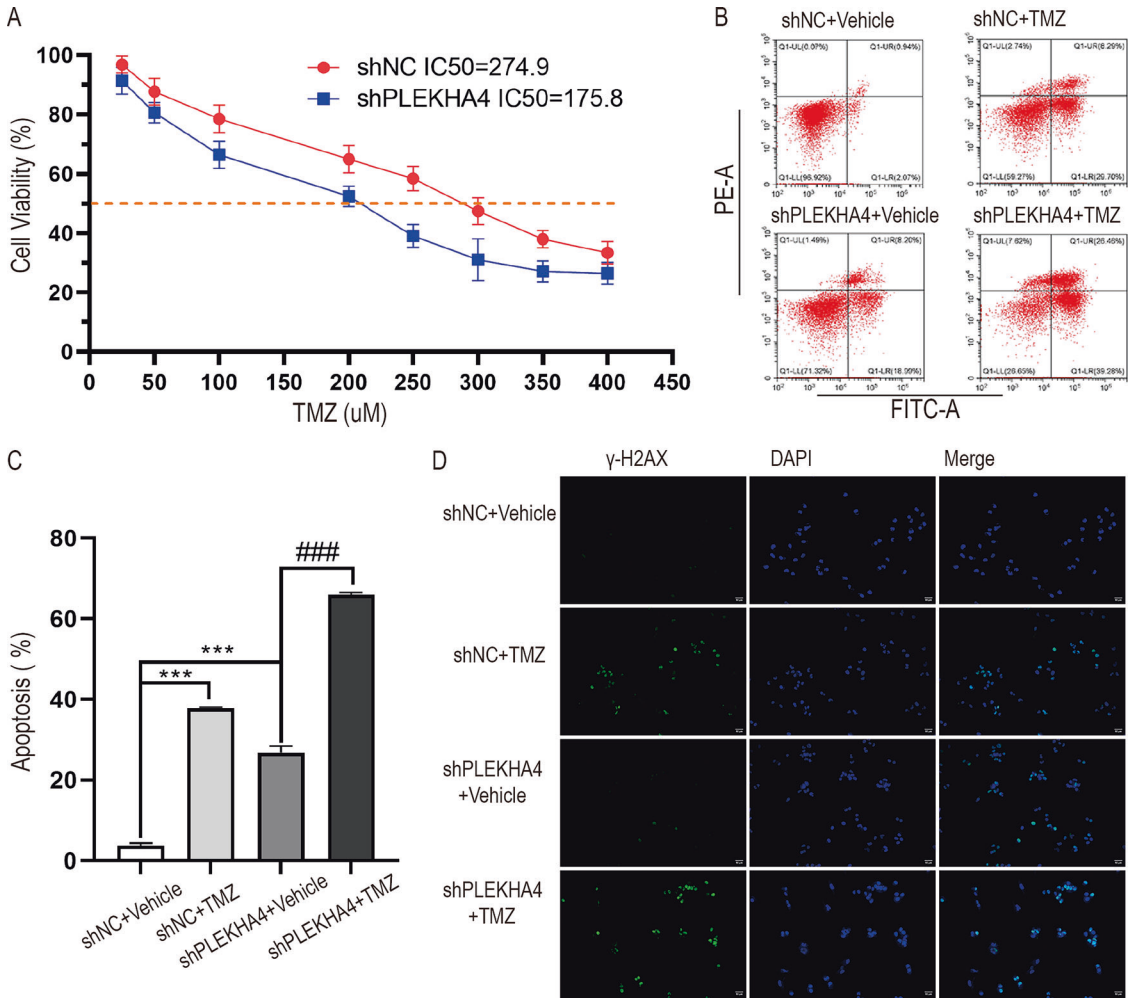

Fig. 8 TMZ promoted the apoptotic effect of *PLEKHA4* in glioma cells. A CCK8 detected the effect of different concentrations of TMZ on cell viability (shNC IC 50 = 274.9; sh*PLEKHA4* IC 50 = 175.8). **B** Flow cytometry detected cell apoptosis. **C** The quantitative analysis of cell apoptosis. ***$p < 0.001$ compared with shNC + Vehicle, ###$p < 0.001$ compared with sh*PLEKHA4* + TMZ group. **D** Immunofluorescence detected the expression of *γ-H2AX*. The cell experiments were conducted three independent cultures, with two replicates conducted each time.

Expression Profiling Interactive Analysis), which comprised data from glioma and normal tissues. *PLEKHA4* expression was analyzed in glioma and non-glioma tissues.

Gene set enrichment analysis (GSEA)

GSEA (http://www.broad.mit.edu/gsea/) was used to assess the correlation between *PLEKHA4* expression and biological processes/pathways. We divided the dataset obtained from TCGA into two groups (high and low *PLEKHA4* expression). We select default settings, analyzed the data to determine significance thresholds, and calculated the FDR. It is generally believed that an Enrichment fraction (NES) with $|NES| > 1$, $p < 0.05$, and a q-value (i.e. FDR) < 0.25 is considered substantially enriched.

Cell culture

The human GBM cell lines, such as T98G were acquired from the BeNa Culture Collection (BNCC, Henan, China), U87, U251, and U343 were acquired from Jiandun Biotechnology (Shanghai, China), and HBMECs were acquired from Procell (Wuhan, China). U251, U87, U343, T98G, and HBMECs were cultured in DMEM (Biosharp, Anhui, China) supplemented with 10% fetal bovine serum (FBS, Gibco, USA). Cells were placed in a 5% CO_2 incubator. All cell STR profiling and mycoplasma testing were shown in the supplementary information section.

Lentiviral infection

Three *PLEKHA4* shRNAs were synthesized and cloned using the Plko.1-puro cloning vector. To prepare *PLEKHA4* overexpression, the *PLEKHA4* sequence was sub-cloned into the Plvx-Puro lentiviral vector. T98G and U87 cells were infected with shRNA-expressing and overexpressing lentiviral supernatants, and after 72 h of infection, mRNA and protein expression was determined. The shRNA sequences were as follows:

shRNA-1: 5′-GGAGAAGGAGCAACTAGAA-3′, 5′-TTCTAGTTGCTCCTTCTCC-3′;
shRNA-2: 5′-GCTACAATCCAGCTTCTAA-3′, 5′-TTAGAAGCTGGATTGTAGC-3′;
shRNA-3: 5′-GAGTCAACTTTCCACCAAA-3′, 5′-TTTGGTGGAAAGTTGACTC-3′

qRT-PCR

TRIzol (YEASEN, Shanghai, China) was used to collect total RNA. Complementary DNA was reversed transcribed with the Hifair® II 1st strand cDNA Synthesis Kit (YEASEN, Shanghai, China), per the manufacturer's instructions. Transcripts were amplified via qPCR using the Hieff® qPCR SYBR Green Master Mix (YEASEN, Shanghai, China). *HOXD9* and *PLEKHA4* primer sequences were as follows:

HOXD9: F 5′ -TTTGGGGTTTCGCCCTATCC-3′, R 5′ - CTGGGGGTGAGGGGACTAAA-3′;
PLEKHA4: F 5′ - TGTCCGACCTCCTCTGGATT-3′, R 5′ - AGAGTGTGCCTGTGTTCTGG-3′;
Actin: F 5′ -CCTTCCTTCCTGGGCATGG-3′, R 5′ - GATCTTCATTGTGCTGGGTGC-3′.

Western blotting

Total protein was extracted from cells, and quantified using BCA kit. Then 20 μg of protein were added to the a 10% SDS-PAGE gel for electrophoresis, after which the protein was transferred to 0.22 μm PVDF membranes. The membranes were removed and placed in 5% nonfat milk

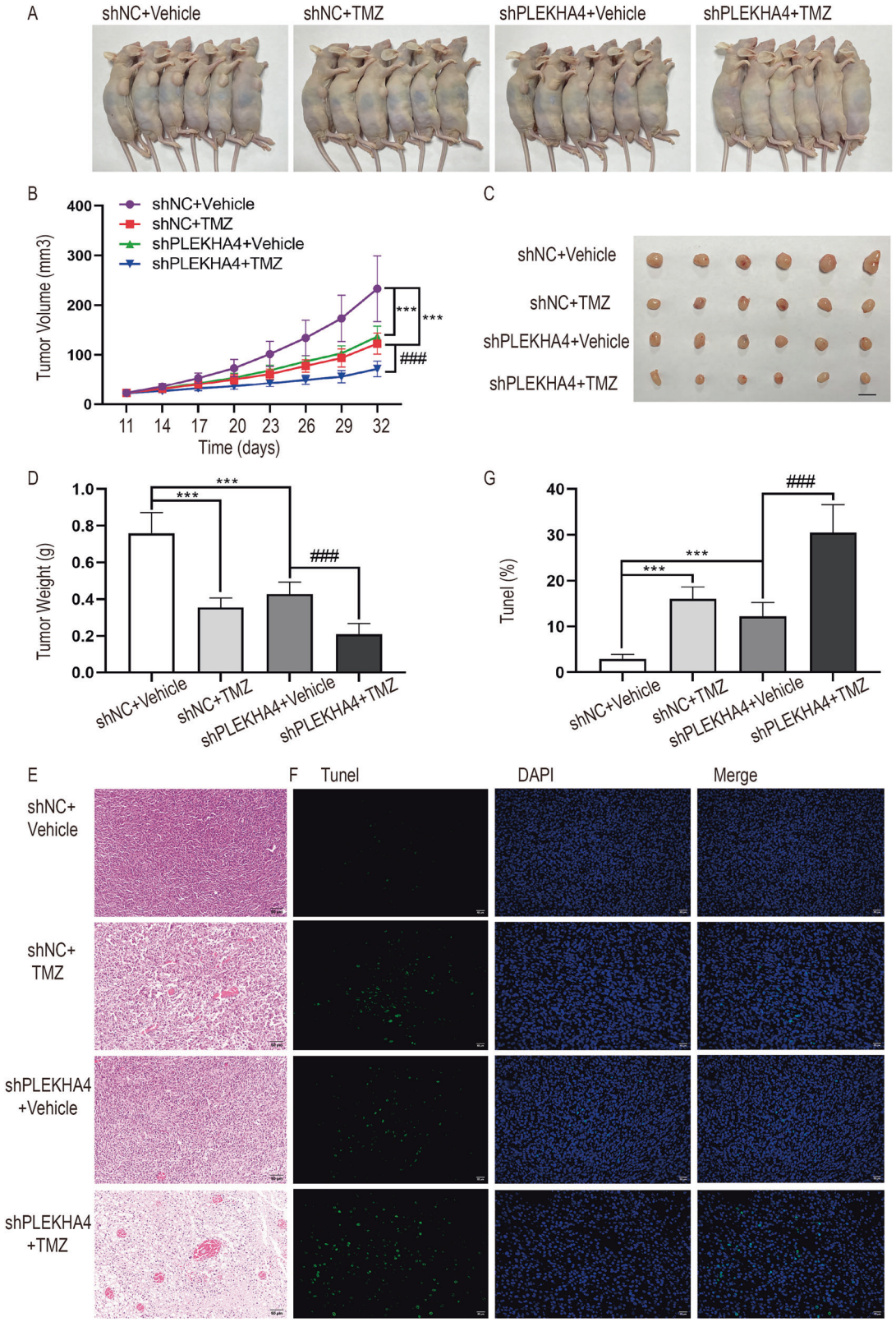

Fig. 9 TMZ combined with *PLEKHA4* knockdown to inhibit tumor growth and apoptosis in subcutaneous transplant tumor model. A The images of subcutaneous transplant tumors, were divided into four groups: shNC + Vehicle; shNC + TMZ; sh*PLEKHA4* + Vehicle; sh*PLEKHA4* + TMZ. **B** Tumor growth curve. ***$p < 0.001$ compared with shNC + Vehicle group, ###$p < 0.001$ compared with shNC + TMZ group. **C** Tumor size and **D** Tumor weight. ***$p < 0.001$ compared with control group, ###$p < 0.001$ compared with shNC + TMZ group. **E** HE staining. **F** Tunel staining. **G** The quantitative analysis of TUNEL. ***$p < 0.001$ compared with control group, ###$p < 0.001$ compared with shNC +TMZ group.

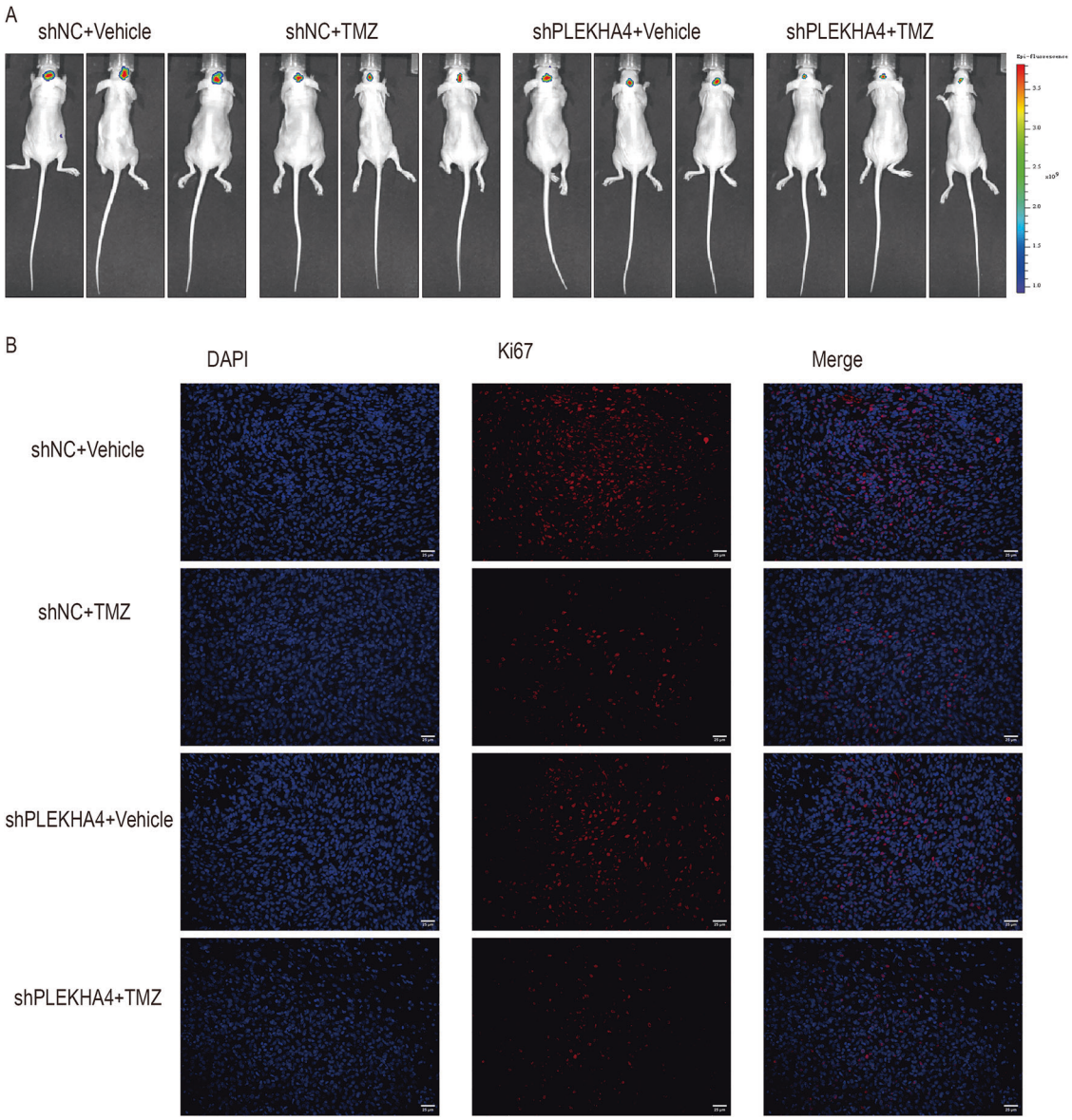

Fig. 10 TMZ combined with *PLEKHA4* knockdown to inhibit tumor growth in intracranial model. A The image of intracranial tumor. **B** Immunofluorescence detected the expression of *Ki67* (400×).

for blocking, followed by incubation with primary antibodies overnight at dilutions of 1:5000 (anti-*PLEKHA4*; Abcam, Ab84727, UK), 1:2000 (anti-*HOXD9*; CST, 55962, USA), 1:2000 (anti-*STAT3*; Abcam, Ab119352, UK), 1:3000 (anti-*p-STAT3*; Abcam, Ab76315, UK), 1:1000 (anti-*SOCS1*; Abcam, Ab280886, UK), and 1:5000 (anti-*β-actin*; Proteintech, 66009-1-Ig, Wuhan China). Subsequently, an HRP-conjugated secondary antibody at a dilution of 1:10000 (Goat anti-mouse; ZSGB-BIO, ZB-2305, Beijing, China) or (Goat anti rabbit; ZSGB-BIO, ZB-2301, Beijing, China) was incubated for 1 h at 37 °C. ECL chemiluminescence detected the protein expression, which was quantified using Image J software (National Institutes of Health, USA).

Reagents

TMZ (MCE, HY-17364, china) was purchased from MedChemExpress (MCE, https://www.medchemexpress.cn/). We prepared a 10 mM TMZ solution with dimethyl sulfoxide (DMSO) and separated it to avoid repeated freeze-thaw cycles. It was stored at −20 °C. All antibody information was shown in Table S1.

Cell proliferation

Cell Counting Kit-8 (CCK8, Beyotime, C0039, China) was used to detect cell growth per the manufacturer's instructions. An aliquot of the 5×10^3 cell suspension was added in triplicate to a 96-well plate and grown at 37 °C. Add 10 μl CCK8 reagents into each well at 0, 12, 24, 48, and 72 h of incubation, followed by incubation at 37 °C for 1.5 h. The absorbance was measured at 450 nm using an enzyme label analyzer (PERLONG, DNM-9602, Beijing, China).

Cell apoptosis

The Annexin V-FITC staining kit (Beyotime, Shanghai, China) was used to detect GBM cell apoptosis. According to the manufacturer's instructions, we collected cells and re-suspended them with a staining solution, followed by incubation them with annexin V-FITC and Propidium Iodide (PI) in the dark for 15 min. A Calibur Flow Cytometer (Beckman, CytoFLEX, USA) was used to detect apoptosis, where Annexin V^+/PI^- cells were deemed to be early apoptotic cells.

Glucose uptake assays

We collected cells to detect glucose uptake. The cells were incubated in a culture medium containing 2-NBDG (2-(N-(7-nitrobenz-2-oxa-1,3-dizol-4-yl) amino)-2-deoxyglucose, Bio Vision, USA). After incubation, the cells were collected and centrifuged, re-suspended with PBS, and finally analyzed with FlowLogic FCS analysis software (Backman Coulter, USA).

ATP and lactate assays

ATP and lactate were measured using the ATP and lactate kits (Nanjing Jian-cheng Bioengineering, Nanjing, China). After transfecting T98G or U87 cells with *PLEKH4A*-shRNA or the *PLEKHA4* overexpression vector, the cells were collected. The assays were conducted according to the instructions of the kit. Finally, the fluorescence microplate reader (BioTek, SYNERGY H1) was used for detection. ATP and lactate concentrations were computed using the following formula:

$$\mathrm{ATP}\,(\mu\mathrm{mol/gprot}) = (\mathrm{OD_{test}} - \mathrm{OD_{control}})/(\mathrm{OD_{standard}} - \mathrm{OD_{zero}}) \times \text{standard sample} \times (\text{dilution multiple/protein concentration})$$

$$\text{Lactic acid}(\mathrm{mM}) = (\mathrm{OD_{test}} - \mathrm{OD_{zero}})/(\mathrm{OD_{standard}} - \mathrm{OD_{zero}}) \times \text{standard sample} \times \text{dilution multiplier}$$

Luciferase reporter assay

The dual-luciferase *PLEKHA4* and HOXD9 overexpression vectors were co-transfected into U87 cells. After 48 h, the relative luciferase activity and Renilla luciferase activity were detected, and the obtained data were analyzed and processed to obtain the differences between experimental and control group. All samples were detected in triplicates.

Immunofluorescence

Cells were fixed with 4% formaldehyde for 30 min, permeabilized with 0.5% Triton X-100 for 10 min, blocked with 1% BSA for 1 h, and incubated with primary antibody (anti-*γ-H2AX*, Abcam, Ab81299, 1:100, UK) at 4 °C overnight. Then, we added the diluted fluorescent secondary antibody (Alexa Fluor 488-labeled goat-Rabbit IgG (H + L), Beyotime, A0423, China) and incubated the cells for 1 h. Finally, the cells were treated with a mixture of anti-quenching sealing agent and DAPI, followed by imaging under a fluorescence microscope. The cell nucleus was dyed blue, and the positive results were dyed green.

Xenograft models

Eighteen male nude mice (18–22 g, 6 weeks old) were procured from Hangzhou Ziyuan Experimental Animal Technology Company (Hangzhou, China). The animals were retained at 22 ± 1 °C, under a 12 h light-dark cycle, and provided water ad libitum. Mice were randomly divided into three groups: shNC, sh*PLEKHA4-1* and sh*PLKHA4-3* groups ($n = 6$ per group), with 2×10^6 T98G cells injected into each mouse in their left axilla. Once the tumor grew, the tumor's length and width were measured to calculate its volume every three days. After 33 days, the mice were euthanized, and the tumors were removed and weighed. The volume was calculated based on the measured length and width, along with the growth curve. Tumor volume (mm^3) = 0.5 × length × $width^2$.

Twenty-four nude mice were randomly divided into four groups (shNC + Vehicle, shNC + TMZ, sh*PLEKHA4* + Vehicle, sh*PLEKHA4* + TMZ) and inoculated with T98G-shNC or T98G-*shPLEKHA4* stable transgenic cell lines ($n = 6$ per group). Then, 2×10^6/200 μl cell suspension was subcutaneously injected into the right forearm axilla of nude mice. After inoculation, different groups of nude mice were raised in cages, regularly fed with water and feed, and the bedding was changed regularly. One week later, the shNC + TMZ and sh*PLEKHA4* + TMZ groups were injected with TMZ (50 mg/kg) via intraperitoneal injection for five consecutive days, while the remaining groups were injected with an equal amount of solvent (intraperitoneal injection). Then, we measured the size of the tumor with a caliper every three days. After the administration, each group of experimental mice was euthanized, and the tumors were immediately removed and imaged. We weighed the tumor and measured the volume, then we fixed the tumor in 4% paraformaldehyde to prepare it for subsequent sectioning and pathology.

Intracranial models

6-week-old female Balb/c nude mice were used to construct an in intracranial model of glioma. The experimental process is as follows: 1×10^6 U87 cells stably expressing firefly luciferase (Fluc) were injected into the mouse brain 2 mm laterally, 2 mm posteriorly, and 2 mm deep using a stereotactic device. 10 days after implantation, small animal imaging was performed to confirm tumor occurrence, the mice were randomly divided into eight groups ($n = 3$ per group), then STAT3 inhibitor AG490 was administered via intraperitoneal injection every 2 days for 2 groups, and then intraperitoneal injection of TMZ (25 mg/kg) every 2 days for 2 groups, intraperitoneal injection of the same volume of solvent for other groups. The experimental groups are as follows: Vector + Vehicle, Vector + AG490, oePLEKHA4 + Vehicle, oePLEKHA4 + AG490, shNC + Vehicle, shNC + TMZ, shPLEKHA4 + Vehicle, shPLEKHA4 + TMZ.

IVIS imaging

Fluorescent drugs were injected into every mouse via intraperitoneal injection, after injection, the mice were anesthetized with isoflurance (RWD, China) at a set time point, then performed live fluorescence imaging using a small animal live imaging device (IVIS Lumina LT Series III, USA). The data were analyzed with the IVIS software (Living Imaging Software for IVIS).

Hematoxylin and Eosin (HE) staining

The tumor tissues were embedded in paraffin blocks and cut into 5 μm thick sections. The paraffin sections were baked for 45 min and placed in xylene I, xylene II and xylene III solution for dewaxing. The dewaxed sections were then hydrated in gradient alcohol (alcohol concentration: 100%, 95%, 85%, and 75%) for 5 min each. Then, we performed HE staining, controlling the staining time. Finally, we observed and imaged the sections under a microscope, and analyzed the collected images.

Immunofluorescence

The tumor tissues were embedded in paraffin blocks and cut into 5 μm thick sections. The sections were baked for 45 min and deparaffinized them in xylene I, xylene II and xylene III solution for 10 min each. Then placed in gradient alcohol (100%, 95%, 85%, and 75% alcohol concentration) for 5 min each. Then, antigen repair was performed using a 0.02 M sodium citrate buffer solution at high temperature for 15 min. Incubated with primary antibody (*Ki67*, proteintech, 27309-1-AP, 1:100, China) at 4 °C overnight. Incubated the fluorescent secondary antibody (Alexa Fluor 555-labeled donkey-rabbit IgG (H + L), Beyotime, A0453, China) at room temperature for 1 h. The sections were Sealed with DAPI containing quenching sealing agent. Immunofluoresence microscopy observation and photography (400×).

Tunel staining

We embeded the tumor tissues in paraffin blocks, and cut them into 5 μm thick sections. We baked and dewaxed the sections separately, and then TUNEL staining (Roche, 11684817910, Switzerland) was performed. The sections were incubated at 37 °C for 1 h, followed by staining and sealing with a mixture of anti-quenching sealing agent and DAPI. Finally, we observed and imaged the sections under a fluorescence microscope, and we analyzed the collected images to calculate the apoptosis rate.

Statistical analysis

All the data were presented as mean ± SD. Groups differences were determined using repeated ANOVA tests followed by Bonferroni correction and Student's t-tests. Statistical significance was set at $P < 0.05$. For cell experiments such as qPCR, Western blotting, cell proliferation and cells apoptosis, we conducted three independent cultures. In each independent culture, we conducted 3 repeated experiments to evaluate the reproducibility of the experiment.

DATA AVAILABILITY

The original contributions presented in the study are included in the article, further inquiries can be directed to the corresponding author.

REFERENCES

1. Yang R, Wang M, Zhang G, Li Y, Wang L, Cui H. POU2F2 regulates glycolytic reprogramming and glioblastoma progression via PDPK1-dependent activation of PI3K/AKT/mTOR pathway. Cell Death Dis. 2021;12:433. https://doi.org/10.1038/s41419-021-03719-3.
2. Zeng J, Zhang J, Yang YZ, Wang F, Jiang H, Chen HD, et al. IL13RA2 is overexpressed in malignant gliomas and related to clinical outcome of patients. Am J Transl Res. 2020;12:4702–14.
3. Liu X, Yue C, Shi L, Liu G, Cao Q, Shan Q, et al. MALT1 is a potential therapeutic target in glioblastoma and plays a crucial role in EGFR-induced NF-κB activation. J Cell Mol Med.2020;24:7550–62. https://doi.org/10.1111/jcmm.15383.

4. Aldape K, Zadeh G, Mansouri S, Reifenberger G, von Deimling A. Glioblastoma: pathology, molecular mechanisms and markers. Acta Neuropathol. 2015;129:829–48. https://doi.org/10.1007/s00401-015-1432-1.
5. Sturm D, Pfister SM, Jones DTW. Pediatric gliomas: current concepts on diagnosis, biology, and clinical management. Journal Clin Oncol: Off J Am Soc Clin Oncol. 2017;35:2370–7. https://doi.org/10.1200/jco.2017.73.0242.
6. Lee E, Yong RL, Paddison P, Zhu J. Comparison of glioblastoma (GBM) molecular classification methods. Semin Cancer Biol. 2018;53:201–11. https://doi.org/10.1016/j.semcancer.2018.07.006.
7. Tan C, Wei J, Li Z, Tian N, Wang Z, Wang G, et al. Circ_0021350 plays an oncogene role by regulating miR-1207-3p/PIK3R3 in glioblastoma. BMC Cancer. 2023;23:808. https://doi.org/10.1186/s12885-023-11263-w.
8. Van Meir EG, Hadjipanayis CG, Norden AD, Shu HK, Wen PY, Olson JJ. Exciting new advances in neuro-oncology: the avenue to a cure for malignant glioma. CA Cancer J Clin. 2010;60:166–93. https://doi.org/10.3322/caac.20069.
9. Stupp R, Mason WP, van den Bent MJ, Weller M, Fisher B, Taphoorn MJ, et al. Radiotherapy plus concomitant and adjuvant temozolomide for glioblastoma. New Engl J Med. 2005;352:987–96.
10. Qi J, Sun H, Zhang Y, Wang Z, Xun Z, Li Z, et al. Single-cell and spatial analysis reveal interaction of FAP(+) fibroblasts and SPP1(+) macrophages in colorectal cancer. Nat Commun. 2022;13:1742. https://doi.org/10.1038/s41467-022-29366-6.
11. Li BO, Meng C, Zhang X, Cong D, Gao X, Gao W, et al. Effect of photodynamic therapy combined with torasemide on the expression of matrix metalloproteinase 2 and sodium-potassium-chloride cotransporter 1 in rat peritumoral edema and glioma. Oncol Lett. 2016;11:2084–90. https://doi.org/10.3892/ol.2016.4210.
12. Shami Shah A, Batrouni AG, Kim D, Punyala A, Cao W, Han C, et al. PLEKHA4/kramer attenuates dishevelled ubiquitination to modulate wnt and planar cell polarity signaling. Cell Rep. 2019;27:2157–70.e8. https://doi.org/10.1016/j.celrep.2019.04.060.
13. Zhang W, Li L, Bian PP, Luo QP, Xiong ZT. PLEKHA4 is a prognostic biomarker and correlated with immune infiltrates in glioma. Biomed Res Int. 2023;2023:4504474. https://doi.org/10.1155/2023/4504474.
14. Hruz T, Laule O, Szabo G, Wessendorp F, Bleuler S, Oertle L, et al. Genevestigator v3: a reference expression database for the meta-analysis of transcriptomes. Adv Bioinforma. 2008;2008:420747. https://doi.org/10.1155/2008/420747.
15. Shami Shah A, Cao X, White AC, Baskin JM. PLEKHA4 Promotes Wnt/beta-Catenin Signaling-Mediated G(1)-S transition and proliferation in melanoma. Cancer Res. 2021;81:2029–43. https://doi.org/10.1158/0008-5472.CAN-20-2584.
16. Fang C, Liu Y, Chen L, Luo Y, Cui Y, Zhang N, et al. α-Hederin inhibits the growth of lung cancer A549 cells in vitro and in vivo by decreasing SIRT6 dependent glycolysis. Pharmaceutical Biol. 2021;59:11–20. https://doi.org/10.1080/13880209.2020.1862250.
17. Ponnusamy L, Natarajan SR, Manoharan R. MARK2 potentiate aerobic glycolysis-mediated cell growth in breast cancer through regulating mTOR/HIF-1α and p53 pathways. J Cell Biochem. 2022;123:759–71. https://doi.org/10.1002/jcb.30219.
18. Staudt LM, Clerc RG, Singh H, LeBowitz JH, Sharp PA, Baltimore D. Cloning of a lymphoid-specific cDNA encoding a protein binding the regulatory octamer DNA motif. Science. 1988;241:577–80. https://doi.org/10.1126/science.3399892.
19. Agnihotri S, Zadeh G. Metabolic reprogramming in glioblastoma: the influence of cancer metabolism on epigenetics and unanswered questions. Neuro Oncol. 2016;18:160–72. https://doi.org/10.1093/neuonc/nov125.
20. Vander Heiden MG, Cantley LC, Thompson CB. Understanding the Warburg effect: the metabolic requirements of cell proliferation. Science. 2009;324:1029–33. https://doi.org/10.1126/science.1160809.
21. Li X, Wenes M, Romero P, Huang SC, Fendt SM, Ho PC. Navigating metabolic pathways to enhance antitumour immunity and immunotherapy. Nat Rev Clin Oncol. 2019;16:425–41. https://doi.org/10.1038/s41571-019-0203-7.
22. Kesarwani P, Kant S, Prabhu A, Chinnaiyan P. The interplay between metabolic remodeling and immune regulation in glioblastoma. Neuro Oncol. 2017;19:1308–15. https://doi.org/10.1093/neuonc/nox079.
23. Fan Y, Mao R, Yang J. NF-kappaB and STAT3 signaling pathways collaboratively link inflammation to cancer. Protein Cell. 2013;4:176–85. https://doi.org/10.1007/s13238-013-2084-3.
24. Taniguchi K, Karin M. NF-kappaB, inflammation, immunity and cancer: coming of age. Nat Rev Immunol. 2018;18:309–24. https://doi.org/10.1038/nri.2017.142.
25. Yoo SA, Kim M, Kang MC, Kong JS, Kim KM, Lee S, et al. Placental growth factor regulates the generation of T(H)17 cells to link angiogenesis with autoimmunity. Nat Immunol. 2019;20:1348–59. https://doi.org/10.1038/s41590-019-0456-4.
26. Wang Y, Huang J, Zhang F, Shen K, Qiu B. Knock-down of IGFBP2 ameliorates lung fibrosis and inflammation in rats with severe pneumonia through STAT3 pathway. Growth factors (Chur, Switz). 2023;41:210–20. https://doi.org/10.1080/08977194.2023.2259497.
27. Wang Y, Yang C, Sims MM, Sacher JR, Raje M, Deokar H, et al. SS-4 is a highly selective small molecule inhibitor of STAT3 tyrosine phosphorylation that potently inhibits GBM tumorigenesis in vitro and in vivo. Cancer Lett. 2022;533:215614. https://doi.org/10.1016/j.canlet.2022.215614.
28. Ding Z, Kloss JM, Tuncali S, Tran NL, Loftus JC. TROY signals through JAK1-STAT3 to promote glioblastoma cell migration and resistance. Neoplasia. 2020;22:352–64. https://doi.org/10.1016/j.neo.2020.06.005.
29. Pernía O, Sastre-Perona A, Rodriguez-Antolín C, García-Guede A, Palomares-Bralo M, Rosas R, et al. A novel role for the tumor suppressor gene ITF2 in tumorigenesis and chemotherapy response. Cancers. 2020;12:786. https://doi.org/10.3390/cancers12040786.
30. Li ZG, Xiang WC, Shui SF, Han XW, Guo D, Yan L. 11 Long noncoding RNA UCA1 functions as miR-135a sponge to promote the epithelial to mesenchymal transition in glioma. J Cell Biochem. 2020;121:2447–57. https://doi.org/10.1002/jcb.29467.
31. Hirao N, Iwata T, Tanaka K, Nishio H, Nakamura M, Morisada T, et al. Transcription factor homeobox D9 is involved in the malignant phenotype of cervical cancer through direct binding to the human papillomavirus oncogene promoter. Gynecol Oncol. 2019;155:340–8. https://doi.org/10.1016/j.ygyno.2019.08.026.
32. Wen D, Wang L, Tan S, Tang R, Xie W, Liu S, et al. HOXD9 aggravates the development of cervical cancer by transcriptionally activating HMCN1. Panminerva Med. 2022;64:532–6. https://doi.org/10.23736/s0031-0808.20.03911-7.
33. Wu W, Klockow JL, Zhang M, Lafortune F, Chang E, Jin L, et al. Glioblastoma multiforme (GBM): An overview of current therapies and mechanisms of resistance. Pharmacol Res. 2021;171:105780. https://doi.org/10.1016/j.phrs.2021.105780.
34. Ghosh D, Nandi S, Bhattacharjee S. Combination therapy to checkmate Glioblastoma: clinical challenges and advances. Clin Transl Med. 2018;7:33. https://doi.org/10.1186/s40169-018-0211-8.
35. Gao Z, Xu J, Fan Y, Qi Y, Wang S, Zhao S, et al. PDIA3P1 promotes Temozolomide resistance in glioblastoma by inhibiting C/EBPbeta degradation to facilitate proneural-to-mesenchymal transition. J Exp Clin Cancer Res. 2022;41:223 https://doi.org/10.1186/s13046-022-02431-0.
36. Wu Y, Franzmeier S, Liesche-Starnecker F, Schlegel J. Enhanced sensitivity to ALDH1A3-dependent ferroptosis in TMZ-resistant glioblastoma cells. Cells. 2023;12:2522. https://doi.org/10.3390/cells12212522.

AUTHOR CONTRIBUTIONS

Dainan Zhang: Writing – review & editing, Visualization, Project administration. Xiaoyin Wang: Writing – original & draft, Data curation, Visualization. Meng Xiao: Software, Data curation, Visualization. Shunchang Ma: Data curation, Data curation, Visualization. Shaomin Li: Writing – review & editing, Formal analysis, Conceptualization. Wang Jia: Writing – review & editing, project administration, Conceptualization.

FUNDING

This study was supported by National Key R&D Program of China (No.2022YFF0608404), Henan Key Laboratory of Neural Regeneration and Repairment (No.HNSJXF-2021-001), and Medical Science and Technology Key Project in Henan Province (No.222102310693).

COMPETING INTERESTS

The authors declare no competing interests.

ETHICS

This study was approved by the Experimental Animal Committee of Beijing Tiantan Hospital Capital Medical University (KY-2022-048-01). All methods were performed in accordance with the relevant guidelines and reVgulations.

ADDITIONAL INFORMATION

Supplementary information The online version contains supplementary material available at https://doi.org/10.1038/s41389-025-00559-0.

Correspondence and requests for materials should be addressed to Wang Jia.

Reprints and permission information is available at http://www.nature.com/reprints

Publisher's note Springer Nature remains neutral with regard to jurisdictional claims in published maps and institutional affiliations.